Eigenmode Distortion: A New Perspective on Motion Cueing Fidelity in Flight Simulation

Miletović, I.; Pavel, M.D.; Pool, D.M.; Stroosma, O.; van Paassen, M.M.; Mulder, Max; Wentink, Mark

Citation (APA)
Miletović, I., Pavel, M. D., Pool, D. M., Stroosma, O., van Paassen, M. M., Mulder, M., & Wentink, M. (2021). Eigenmode Distortion: A New Perspective on Motion Cueing Fidelity in Flight Simulation. *Journal of Guidance, Control, and Dynamics: devoted to the technology of dynamics and control*, *44*(7), 1314-1326. https://doi.org/10.2514/1.G005596

Important note
To cite this publication, please use the final published version (if applicable).
Please check the document version above.

Eigenmode Distortion: A New Perspective on Motion Cueing Fidelity in Flight Simulation

Ivan Miletović,* Marilena D. Pavel,† Daan M. Pool,‡ Olaf Stroosma,*
Marinus M. van Paassen,† and Max Mulder§
Delft University of Technology, 2629 HS Delft, The Netherlands
and
Mark Wentink¶
Desdemona B.V., 3769 DE Soesterberg, The Netherlands

Eigenmode distortion is a novel quantitative methodology developed to objectively evaluate motion cueing fidelity in flight simulation. It relies on an explicit coupling of linearized vehicle and Motion Cueing Algorithm dynamics. Modal analysis subsequently performed on this coupled system reveals the degree of *distortion* imposed by the Motion Cueing Algorithm on to the dynamics of the simulated vehicle. Eigenmode distortion thereby provides unprecedented insight into the combined dynamics of the two systems along modal coordinates. Compared with existing methods for motion cueing fidelity assessment, the eigenmode distortion method enables a systematic analysis of the coupled vehicle and Motion Cueing Algorithm dynamics. This is mainly because it does not consider the Motion Cueing Algorithm in isolation and does not inherently rely on assumptions regarding the excitation of the simulated vehicle dynamics. This paper outlines the theoretical foundation of the eigenmode distortion method and includes a case study on helicopter longitudinal dynamics and a sensitivity analysis to demonstrate its utility. The results presented in this paper shown that the eigenmode distortion method can reveal interactions between the Motion Cueing Algorithm and the vehicle dynamics that are currently not captured by other established methods, such as the Sinacori–Schroeder criteria and the Objective Motion Cueing Test.

Nomenclature

A, B, C, D	=	linear system state, input, and output matrices
f_x, f_y, f_z	=	specific force, m/s^2
g	=	gravitational acceleration, m/s^2
K_p, K_q, K_r	=	Classical Washout Algorithm motion gains in rotational motion channels
K_x, K_y, K_z	=	Classical Washout Algorithm motion gains in translational motion channels
m_i	=	mode participation factor of ith system mode
p, q, r	=	angular rates expressed in vehicle body-aligned reference frame, rad/s
q	=	auxiliary state vector used in state-space formulation of Motion Cueing Algorithm filters
r	=	state vector expressed in modal coordinates
u	=	input vector
u, v, w	=	velocities expressed in body-aligned reference frame, m/s
V	=	matrix of left eigenvectors corresponding to linear system
W	=	linear system modal matrix
w, v	=	right and left eigenvectors
x	=	state vector
y	=	output vector
$\{X, Y, Z\}_u, \{X, Y, Z\}_v, \{X, Y, Z\}_w$	=	force stability derivatives w.r.t. velocity, 1/s
$\{X, Y, Z\}_p, \{X, Y, Z\}_q, \{X, Y, Z\}_r$	=	force stability derivatives w.r.t. angular velocity, m/(s · rad)
$\{L, M, N\}_u, \{L, M, N\}_v, \{L, M, N\}_w$	=	moment stability derivatives w.r.t. velocity, rad/(s · m)
$\{L, M, N\}_p, \{L, M, N\}_q, \{L, M, N\}_r$	=	moment stability derivatives w.r.t. angular velocity, 1/s
$\delta_0, \delta_{1_s}, \delta_{1_c}, \delta_\theta$	=	collective and cyclic control deflections, % or rad
$\delta\square$	=	linearized quantity
ζ	=	Classical Washout Algorithm filter damping ratio
λ	=	eigenvalue
Φ	=	vector containing Euler attitude angles, rad
ϕ, θ, ψ	=	roll, pitch and yaw attitude angles, rad
$\omega_{1_x}, \omega_{1_y}, \omega_{1_z}$	=	Classical Washout Algorithm filter break frequency in channel 1, rad/s
$\omega_{2_x}, \omega_{2_y}$	=	Classical Washout Algorithm filter break frequency in channel 2, rad/s
$\omega_{3_p}, \omega_{3_q}, \omega_{3_r}$	=	Classical Washout Algorithm filter break frequency in channel 3, rad/s
$\square$	=	generic symbol placeholder

Subscripts

e	=	equilibrium state
1,2,3	=	Classical Washout Algorithm channel number

Superscripts

c	=	quantity pertaining to coupled system formulation

*Researcher, Faculty of Aerospace Engineering, Kluyverweg 1, Section of Control & Simulation.

†Associate Professor, Faculty of Aerospace Engineering, Kluyverweg 1, Section of Control & Simulation.

‡Assistant Professor, Faculty of Aerospace Engineering, Kluyverweg 1, Section of Control & Simulation.

§Full Professor, Faculty of Aerospace Engineering, Kluyverweg 1, Section of Control & Simulation.

¶Technical Director, Kampweg 55.

r	=	quantity expressed in the inertial reference frame
m	=	quantity pertaining to Motion Cueing Algorithm dynamics in coupled system formulation
p	=	quantity pertaining to vehicle dynamics in coupled system formulation
s	=	quantity expressed in the simulator body-aligned reference frame

I. Introduction

HISTORICALLY, qualification of motion cueing systems (MCSs) in full flight simulators (FFSs) used for pilot training relies heavily on subjective assessment by qualified pilots [1]. In fact, currently prescribed regulations stipulate that "until there is an objective procedure for determination of the motion cues necessary [. . .], motion systems should continue to be tuned subjectively" ([1] p. 75).

Over the years, there have been several contributions toward the formulation of more quantitative criteria for motion cueing fidelity assessment. Perhaps the best known are the Sinacori–Schroeder criteria first proposed by Sinacori [2] and later refined by Schroeder [3]. These criteria stipulate acceptable boundaries on motion distortion** in the frequency domain. A decade ago, Advani and Hosman [4,5] proposed a more general approach, the Objective Motion Cueing Test (OMCT), based on the measurement of the linear frequency response of the integrated MCS. The MCS comprises the Motion Cueing Algorithm (MCA) and the motion platform hardware in conjunction with all its associated control laws. OMCT therefore provides insight into the amplitude and phase distortion induced by the MCS, for a range of different sinusoidal motion inputs. After application of the method at various independent institutions and subsequent refinement [6], the International Civil Aviation Authority (ICAO) adopted the test in its manual of criteria for the qualification of flight simulation training devices (FSTDs) in 2009 ([7] II-Att F-1). Currently, a preliminary set of criteria based on industry best practice is available for fixed-wing aircraft FSTD [8] and the FAA requires that the OMCT be applied to all newly qualified simulators [9]. The validation and refinement of the OMCT criteria is an ongoing process and is performed in close cooperation with partners from both academia and industry [10–15].

An important caveat of these frequency-domain methods is that they consider the MCS in isolation and do not explicitly include aircraft- and/or pilot-specific factors. More specifically, in OMCT, vehicle dynamics and pilot control inputs are abstracted to a set of single sines applied to the MCS. These input signals have a fixed set of amplitudes at 12 prescribed frequencies ranging from 0.1 to 15.8 rad/s, with fixed amplitudes considered to be representative. To better represent the conditions the MCS encounters during flight, Dalmeijer et al. [16] extended the OMCT for application in the rotorcraft domain by replacing the fixed sinusoids by signals that more closely resemble a helicopter's behavior in a certain maneuver. They found that rotorcraft-specific (i.e., "tailored") OMCT input signals are able to expose interactions in motion cueing signals that are not captured in the present OMCT. Nonetheless, the signals remain specific to a combination of vehicle and task. A change in either requires a redefinition of the frequency domain data and, hence, might result in substantially different results. Moreover, processing of the vehicle- and task-specific frequency domain data was shown to be highly sensitive to interpilot variability. Thus, tailored OMCT results remain difficult to generalize across different in vehicles, tasks and pilots, making their use as a qualification test unfeasible. The method proposed in this paper will address these issues.

Despite its limitations, OMCT has proven to be a well-established and valuable tool to gain broad insight into the dynamic properties of the MCS, particularly in the realm of fixed-wing flight simulation for pilot training and certification. However, some applications may benefit from a more focused approach that foregoes the definition of explicit MCA excitation signals and instead directly leverages knowledge embedded in a vehicle dynamics model. This is a common practice in, e.g., the evaluation of aircraft handling qualities [17], where in conjunction to frequency domain metrics, criteria are specified in terms of time-domain responses and dynamic mode properties (i.e., short period, phugoid, etc.) [18,19]. The novel method proposed in this paper, named *eigenmode distortion* (EMD), aligns particularly well with the latter as it also relies on modal analysis to quantify the effect of the MCA in terms of the *distortion* of the simulated vehicle dynamics. Specifically, it provides insight into the combined simulated vehicle and MCA dynamics along a set of decoupled (i.e., modal) coordinates. Existing applications of modal analysis are vast and span multiple scientific and engineering disciplines. In aerospace, it is perhaps best known for its utility in structural vibration analysis and control [20–22], aerodynamics [23], as well as aircraft stability analysis [24,25] and flight control system design [26–28].

The main contributions of this paper are twofold. First, it presents the theoretical foundation of EMD, which primarily relies on modal analysis, as applicable to any linearizable combination of vehicle and MCA. This also includes an example derivation of the method for the case of six-degree-of-freedom (6-DOF) aircraft motion cued using the well-known Classical Washout Algorithm (CWA) [29]. These mathematical derivations form the basis of earlier work that relies on the EMD method, e.g., [30–32]. Second, the paper aims to demonstrate the applicability of the EMD method. This is accomplished using an example application of EMD using the dynamics of the Bo-105 helicopter, which shows how the method allows new insights to be gained into the coupled dynamics of the simulated vehicle and MCA. In addition, results from a preliminary pilot-in-the-loop experiment [30] are used to introduce the mode participation factor (MPF) as a useful metric to facilitate in task-specific MCA tuning based on EMD.

The paper is structured as follows. First, the technical background regarding the significance of modal analysis is presented in Sec. II, which includes a proposition for a system structure to capture the *coupled* vehicle and MCA dynamics. Then, in Sec. III, the dynamics of a commonly applied MCA, the CWA, are explained and linearized. Section IV subsequently completes the formulation of the coupled system and presents its sought eigenstructure. In Sec. V, a case study and sensitivity analysis is included to exemplify the utility of the novel methodology. Finally, Sec. VI introduces the MPF using results from a preliminary pilot-in-the-loop experiment.

II. Eigenmode Distortion

The EMD method relies on the algebraic coupling of simulated vehicle and MCA dynamics and the subsequent application of modal analysis to the resulting coupled system. Algorithm 1 summarizes the method in three steps. Because modal analysis is at the core of the EMD method, this section first highlights the significance of modes for the analysis of dynamic systems. To that end, Sec. II.A introduces the notion of modes and its relation to the time-domain response of a dynamic system. Then, Sec. II.B outlines the idea of leveraging modal analysis for application to motion cueing fidelity evaluation.

Algorithm 1:   The three steps of the Eigenmode distortion method

Step 1: Obtain a *linear*(ized) model of the vehicle dynamics, containing expressions for the human-perceived quantities (i.e., specific forces and angular rates) either implicitly or explicitly. This model can be derived analytically or can be obtained empirically.

Step 2: Linearize the applicable MCA. Any MCA can be used as long as it can be feasibly linearized.

Step 3: Couple the two separate linear models of the vehicle and MCA dynamics. This coupled model can then be subjected to a modal coordinate transformation in order to extract information on the MCA-induced modal distortion of human-perceived quantities in terms of the vehicle's dynamic modes.

**In terms of phase and magnitude at a frequency of 1 rad/s, where pilot manual control is predominant.

A. System Response in Terms of Eigenmodes

The property that makes modes attractive for the analyses of linear dynamic systems is that they represent the response characteristics of the system along decoupled coordinates [33]. These coordinates are often collectively termed the "modal coordinates," the "eigenstructure," or, simply, the "modes of the system." Any motion can be described by a combination of modes, and an undisturbed system will continue along its excited modes. As such, the modes provide a more natural representation of a system's state and its evolution as compared with, e.g., more synthetic Fourier coefficients used by OMCT. This section will show how the modes of a generic linear system can be retrieved and how modes are related to the dynamic response characteristics of the system.

Given a linear, nonsingular, and time-invariant system of order n in the form

$$\dot{x} = Ax + Bu$$
$$y = Cx \qquad (1)$$

one can define a transformation of the state vector, x, i.e.,

$$x = Wr \qquad (2)$$

such that

$$\dot{r} = W^{-1}AWr + W^{-1}Bu$$
$$y = CWr \qquad (3)$$

The system in Eq. (3) is said to be *similar* to the one in Eq. (1), in the sense that the dynamic characteristics of the system are unaffected. In fact, the input–output relation from u and y remains unchanged. This furthermore holds for any (nonsingular) choice of the transformation matrix W. However, a special choice for W exists such that [33]

$$W^{-1}AW = \Lambda = \mathrm{diag}(\lambda_1, \lambda_2, \ldots, \lambda_n) = \begin{bmatrix} \lambda_1 & 0 & \cdots & 0 \\ 0 & \lambda_2 & \cdots & 0 \\ \vdots & \vdots & \ddots & \vdots \\ 0 & 0 & \cdots & \lambda_n \end{bmatrix} \qquad (4)$$

In this case, the matrix A is said to be *diagonalized* and $\lambda_1, \ldots, \lambda_i, \ldots, \lambda_n$ are real- or complex-valued scalars known as the *eigenvalues* of the system. In turn, the columns of W, i.e., $w_1, \ldots, w_i, \ldots w_n$, have the property:

$$Aw_i = \lambda_i w_i \quad \text{and} \quad w_i^T \cdot w_j = 0 \quad \forall \, i \neq j \qquad (5)$$

Or, in words, the matrix W is orthogonal and its columns are eigenvectors of the system. W is also often referred to as the *modal matrix*, which effectively decouples the system into its n linearly independent modal coordinates. An individual mode of the system, then, can be uniquely specified as

$$m_i = \{\lambda_i, w_i\} \qquad (6)$$

The type (e.g., stable vs unstable, oscillatory vs nonoscillatory) of the response in a given mode is determined by the eigenvalue associated with that mode. In turn, the eigenvector associated with a mode defines the relative contribution of, and the relation between, the individual states of the system in that mode. This property is commonly referred to as the mode shape.

An example of modes and their corresponding shapes is shown in Fig. 1, depicting the eigenvalues and the associated eigenvectors of a 3-DOF model of the Bo-105 helicopter longitudinal dynamics, in the complex plane. Aircraft modes play an important role in stability and control analysis and design [24,25]. Their prevalence from the early age of aviation has led to well-established names for many common modes.

The typical longitudinal modes for a hingeless helicopter such as the Bo-105 are the pitch subsidence, heave subsidence, and phugoid. Figure 1 shows that the pitch subsidence and heave subsidence are stable aperiodic modes with frequencies of approximately 3.7 and
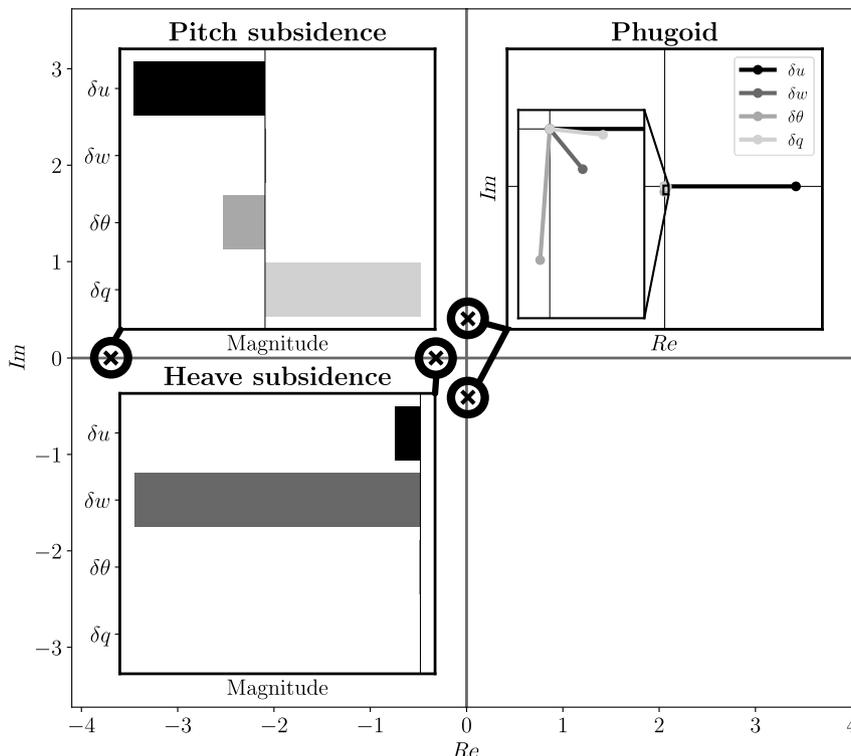

Fig. 1 Eigenvalues of a 3-DOF linear model of the Bo-105 helicopter in hover, depicted in the complex plane, together with the modes they excite in the four state variables.
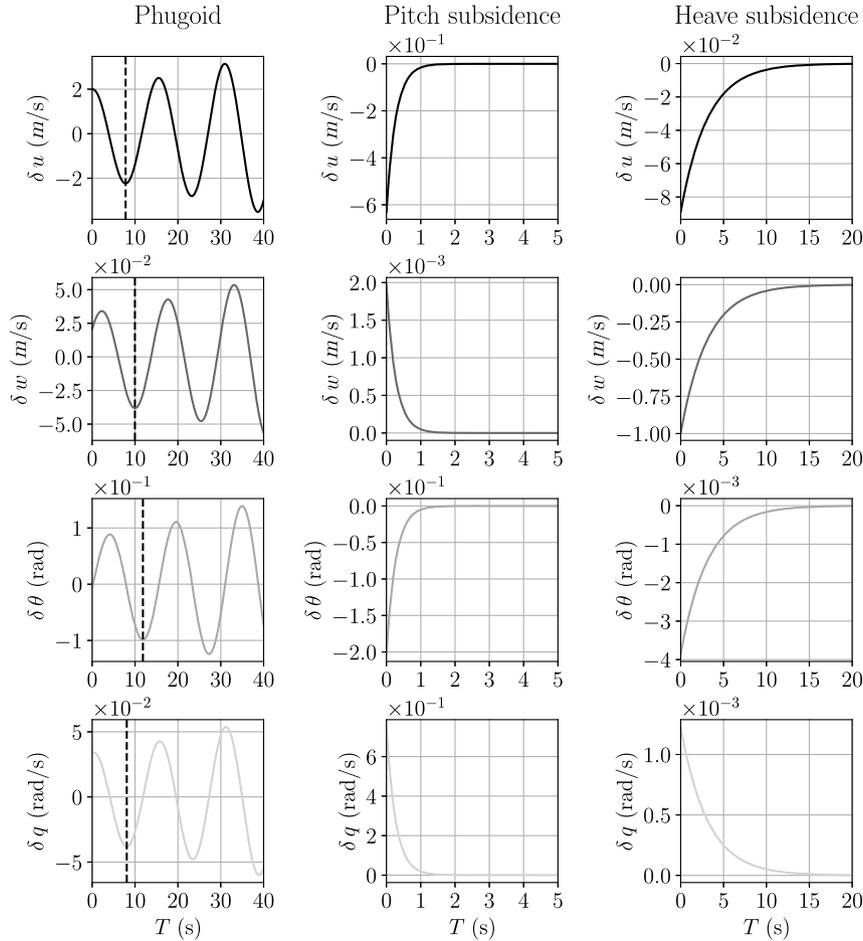
Fig. 2   State responses of isolated modes in a 3-DOF linear model of the Bo-105 in helicopter hover.

0.32 rad/s, respectively. The phugoid is an unstable oscillatory mode with a natural frequency of approximately 0.4 rad/s and a damping ratio of −0.04. Also shown in the figure are the eigenvectors associated with each mode. The elements comprising these eigenvectors are the contributions of the four states in the 3-DOF model in each respective mode. These states are the perturbed velocities along the longitudinal (δu) and vertical (δw) vehicle body axes as well as the perturbed pitch attitude ($\delta\theta$) and rate (δq).

For complex eigenvalues, the corresponding eigenvector coefficients are also complex valued. Hence, each state has a magnitude and phase relative to the other states. This relation is best visualized in a complex plane representation of the eigenvector coefficients. This is illustrated for the phugoid mode in Fig. 1, from which it can be seen that δu is the dominant translational component and $\delta\theta$ is the dominant rotational component. Real eigenvalues are accompanied by real-valued coefficients in the corresponding eigenvectors. In this case, each state has a relative magnitude with respect to other states and is either proportional or inversely proportional to the other states. Thus, the relative relation between real-valued coefficients in an eigenvector can be conveniently represented in a bar plot. This is illustrated in Fig. 1 for the pitch subsidence and heave subsidence modes, where δq and δw, respectively, appear as the dominant contributors. Finally, note that eigenvectors are essentially dimensionless, in that they can be arbitrarily scaled and normalized, and plotted in a dimensionless way (as in Fig. 1). In this process, however, the *relative* relation between the coefficients in each eigenvector is preserved.

The state response of the system is directly related to its modes through [33]:

$$x(t) = \sum_{i=0}^{n} \left[\underbrace{(\boldsymbol{v}_i^T \boldsymbol{x}_0)e^{\lambda_i t}}_{\text{Zero Input Response}} + \underbrace{\int_0^t \boldsymbol{v}_i^T B \boldsymbol{u}(\tau)e^{\lambda_i(t-\tau)}\,d\tau}_{\text{Zero State Response}} \right] \boldsymbol{w}_i \qquad (7)$$

where the row vectors $\boldsymbol{v}_i^T$ are left eigenvectors of the system, which in this case are the rows of a matrix V^T obtained from [††]

$$V^T = W^{-1} \qquad (8)$$

The state response is composed of two parts [see Eq. (7)]. The zero input response (ZIR) captures the contribution to the response due to a direct perturbation of the state itself (i.e., the initial values response). The zero state response (ZSR) only contributes to the response as a result of external inputs. To obtain a response that is isolated to a single system mode, the ZIR corresponding to $\boldsymbol{x}_0 = \boldsymbol{w}_i$ can be evaluated.[‡‡]

An example of ZIRs corresponding to the modes in Fig. 1 is shown in Fig. 2. This figure highlights a number of analogies between the modal domain and the time domain. For example, the responses corresponding to the phugoid mode are unstable and show that δu dominates in terms of amplitude and exhibits *lead* (i.e., precedes in time) with respect to $\delta\theta$ (see dashed lines at first minimum). Also note that all responses in the phugoid mode oscillate with the same frequency. Furthermore, δu and δq appear to be approximately in phase with one another. In Fig. 1, these properties of the response can also be deduced from the relative angle and magnitude between the phugoid eigenvector coefficients in the complex plane. This characteristic lies at the heart of the EMD method. In case of the aperiodic

---

[††]Note that many combinations of V and W exist such that $V^T A W = \Lambda$ and $\boldsymbol{v}_i^T \cdot \boldsymbol{w}_j = 0 \,\forall\, i \neq j$ [33]. Therefore, in contrast to eigenvalues, the left and right eigenvectors of a linear system are generally not unique. The choice $V^T = W^{-1}$ is convenient because it implies that $\boldsymbol{v}_i^T \cdot \boldsymbol{w}_j = 1 \,\forall\, i = j$, which in turn implies that Eq. (7) holds without introducing additional scaling as a result of the implicit inner products of $\boldsymbol{v}_i^T$ and $\boldsymbol{w}_i$.

[‡‡]For periodic modes with complex eigenvectors, the equivalent ZIR is obtained by setting $\boldsymbol{x}_0 = 2Re(\boldsymbol{w}_i)$.

subsidence modes, it can be seen that the further left the eigenvalue lies in the complex plane (i.e., the smaller the time constant), the faster the response.

Given an arbitrary (initial) state or input, Eq. (7) also reveals the extent to which the ith system mode is excited as a result of perturbing the system. This information is present in the terms $\boldsymbol{v}_i^T \boldsymbol{x}_0$ and $\boldsymbol{v}_i^T B\boldsymbol{u}$. Hence, these terms are often referred to as Mode Participation Factors (MPFs) (e.g., [25]). From Eq. (2), one can also directly express a (measured) system state in terms of its modal coordinates using

$$\boldsymbol{r}(t) = W^{-1}\boldsymbol{x}(t) \tag{9}$$

This constitutes an alternative and more complete measure of the participation of each individual system mode in the state response, as it includes the contributions of both the ZIR and ZSR.

B. From Mode Assignment to Distortion

The main contribution of this paper is the application of modal analysis to the problem of motion cueing fidelity in vehicle simulation. An explicit linear(ized) model structure that couples typical (linearized) vehicle and MCA dynamics will be proposed:

$$\delta\dot{\boldsymbol{x}}^c = \begin{bmatrix} A^p & 0 \\ A^{pm} & A^m \end{bmatrix} \begin{bmatrix} \delta\boldsymbol{x}^p \\ \delta\boldsymbol{x}^m \end{bmatrix} + \begin{bmatrix} B^p \\ B^m \end{bmatrix} \delta\boldsymbol{u}^p = A^c\delta\boldsymbol{x}^c + B^c\delta\boldsymbol{u}^p$$

$$\delta\boldsymbol{y}^c = \begin{bmatrix} C^p & 0 \\ C^{pm} & C^m \end{bmatrix} \begin{bmatrix} \delta\boldsymbol{x}^p \\ \delta\boldsymbol{x}^m \end{bmatrix} + \begin{bmatrix} D^p \\ D^m \end{bmatrix} \delta\boldsymbol{u}^p = C^c\delta\boldsymbol{x}^c + D^c\delta\boldsymbol{u}^p \tag{10}$$

The state vectors $\delta\boldsymbol{x}^p$ and $\delta\boldsymbol{x}^m$ that together form the coupled system state $\delta\boldsymbol{x}^c$ in Eq. (10) contain states that describe the evolution of the linearized vehicle and MCA dynamics, respectively. Here, the δ notation is used to emphasize the fact that Eq. (10) describes the *perturbation* dynamics of the coupled vehicle–MCA system. The matrices A^p and A^m are the respective system matrices corresponding to $\delta\boldsymbol{x}^p$ and $\delta\boldsymbol{x}^m$. The matrix A^{pm} couples the dynamics of both systems, whereas the coupled system itself is excited solely by the input vector $\delta\boldsymbol{u}^p$ through the matrices B^p and B^m (combined in the matrix B^c). The matrices A^p and B^p are determined by the pure vehicle dynamics and may change, e.g., as a function of forward flight speed. Conversely, A^m changes purely as a function of parameters in the MCA, whereas A^{mp} and B^m depend on both vehicle dynamics and MCA parameters. For analysis, the coupled system output $\boldsymbol{y}^c$ can be chosen to contain quantities perceived by the human vestibular system (i.e., perception states), both before and after distortion by the MCA. These are specific forces and angular rates [34] that are a linear combination, determined by the matrices C^c and D^c, of the states in $\boldsymbol{x}^p$ and $\boldsymbol{x}^m$.

The key advantage of the formulation in Eq. (10) is that it accommodates modal analysis of the coupled system, as described in Sec. II.A. This is analogous to eigenstructure assignment [28], in the sense that a mechanism is introduced that strongly affects the dynamic properties of the closed-loop system. In eigenstructure assignment, this mechanism (i.e., state feedback) is introduced purposefully with the aim of *shaping* the dynamic characteristics of the closed-loop system. However, in Eq. (10), the presence of the MCA dynamics has the undesired (yet inevitable) side effect of *distorting* the actual vehicle dynamics before being perceived by a human operator in a motion-base flight simulator. The newly proposed method therefore enables a systematic analysis of this MCA-induced distortion of human-perceived quantities in terms of the vehicle's eigenstructure.

In the following sections, the necessary elements in Eq. (10) will be discussed, starting with a linearization of the CWA. In this process, the motion state vector $\boldsymbol{x}^m$ is defined, and expressions for both A^m as well as C^m are obtained. Subsequently, human-perceived quantities (i.e., specific forces and angular rates) will be expressed in terms of the vehicle dynamics states in $\boldsymbol{x}^p$. It will become apparent that these constitute the definition of the A^{pm}, B^m, C^p, C^{pm}, and D^m matrices and thus complete the definition of the coupled system in Eq. (10).

III. Linearizing the Classical Washout Algorithm

From Algorithm 1, it can be seen that obtaining a linear representation of the MCA under consideration is necessary for the application of EMD. This section outlines the process to obtain a linear model of a commonly applied simulator MCA, namely, the CWA [29]. Figure 3 shows a schematic representation of the CWA. This figure shows that the inputs to the CWA are the vehicle specific forces and angular velocities, i.e., the quantities perceived by the human vestibular system [35]. In the CWA, three distinct mechanisms are applied to feasibly reproduce these quantities in the simulator. The purpose of channel 1 is to reproduce high-frequency components of the specific forces. Channel 2 is often referred to as the *tilt coordination* channel, enabling the use of motion platform rotation for reproducing sustained (i.e., low-frequency) specific force components. This channel is optional and only active for specific forces acting in the horizontal plane [29]. Note that tilt coordination introduces an artificial coupling between translational and rotational motion that does not typically exists in, e.g., aircraft dynamics. Finally, channel 3 is responsible for reproducing high-frequency contributions in the angular velocities of the vehicle.

To not divert from the main contributions of this paper, the reader is referred to [36] for the detailed mathematical derivation of the linearized CWA dynamics. However, it is equivalent to that applied elsewhere (e.g., [37]) and the end result relies on a number of
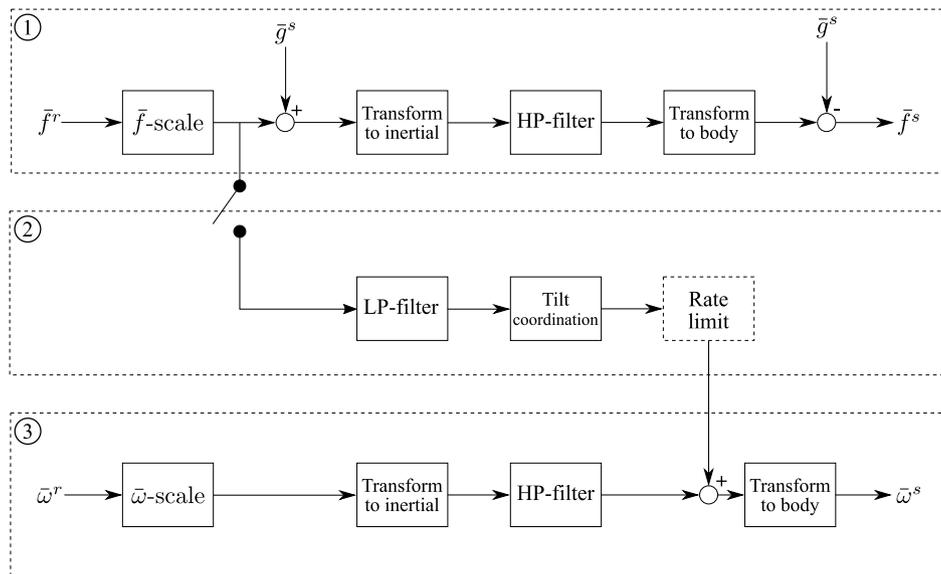

Fig. 3   The three channels of the Classical Washout Algorithm [29].

restrictive yet reasonable assumptions to capture the dynamics of the CWA in 6 DOF in linear form:

1) The CWA is linearized about the neutral state of the simulator, in which the simulator is assumed to be stationary with an attitude equal to zero. This is a reasonable assumption because the CWA itself ensures that the simulator always returns to this state. Moreover, due to mechanical constraints inherent in most conventional contemporary motion platforms, excursions from the neutral position remain relatively small.

2) The vehicle dynamics are linearized with respect to an equilibrium state, which means that (sustained) translational and rotational accelerations are assumed zero in the model. To linearize the CWA, it was furthermore assumed that rotational *rates* of the vehicle in equilibrium are also zero.

3) The rate limit in channel 2 of the CWA is omitted because it cannot be feasibly linearized. However, the (unconstrained) effect of tilt coordination is preserved in the linearization.

Figure 4 summarizes the final schematic obtained for the linearized CWA. It can be seen that, even though many operations have been simplified (e.g., transformations between body and inertial quantities), still many of the inherent interaxis couplings that play a role in EMD remain. Most notably, the rotational dynamics of the CWA in roll and pitch affect the simulated specific forces in sway and surge, respectively, through the addition and subtraction of gravitational components. In turn, the roll and pitch dynamics of the simulator are also influenced by the vehicular specific forces through tilt coordination. The vertical specific force and yaw rate channels, however, do appear as uncoupled DOFs in the linear CWA model.

Figure 4 also shows that the linear dynamics of the CWA are fully determined by a selection of scaling gains, $K_\square$, as well as the various filters $H_{1_\square}$, $H_{2_\square}$ and $H_{3_\square}$. The configurable parameters that appear in these equations are the break frequencies $\omega_{1_\square}$, $\omega_{2_\square}$, and $\omega_{3_\square}$ as well as
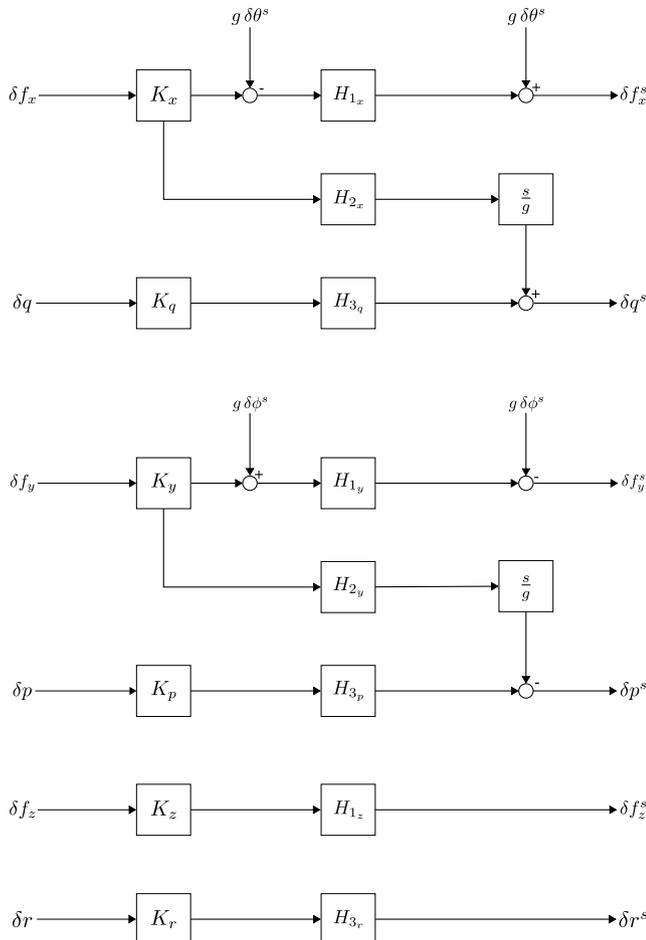

Fig. 4 A schematic of the linearized Classical Washout Algorithm for a full motion simulator.

the common damping ratio ζ. Reflecting back to the coupled model in Eq. (10), it is evident that to capture the linear CWA dynamics, a motion state vector, x^m, can be defined as

$$\delta x^m = \begin{bmatrix} q_{1_x}^T & q_{1_y}^T & q_{1_z}^T & q_{2_x}^T & q_{2_y}^T & q_{3_q}^T & q_{3_r}^T & (\Phi^s)^T \end{bmatrix}^T \quad (11)$$

where $q_{1_\square}$, $q_{2_\square}$, and $q_{3_\square}$ are auxiliary state vectors that appear as a result of the conversion of the CWA filters $H_{1_\square}$, $H_{2_\square}$, and $H_{3_\square}$ to state-space form, and Φ^s is a vector that contains the simulator attitude. The outputs of the linear CWA depicted in Fig. 4 that are of primary interest are the (perturbed) human-perceived specific forces and angular rates. Thus the motion output vector y^m can be defined as

$$\delta y^m = \begin{bmatrix} \delta f_x^s & \delta f_y^s & \delta f_z^s & \delta p^s & \delta q^s & \delta r^s \end{bmatrix}^T \quad (12)$$

Based on the definitions in Eqs. (11) and (12), combined with the results from the CWA linearization [36], it is possible to obtain expressions for the matrices A^m, B^m, and C^m also appearing in Eq. (10). The reader is referred to [36] for the detailed definitions of these matrices.

IV. Obtaining the Coupled System Eigenstructure

The final step in the EMD method, as seen from Algorithm 1, is the coupling of the vehicle and MCA dynamics and the subsequent application of modal analysis to the coupled system eigenstructure. From Fig. 4, it is apparent that the inputs to the CWA are the vehicle perturbed specific forces and rotational rates. This section shows how these quantities can be obtained and expressed in terms of the vehicle dynamics states. This constitutes the last step in the derivation of the coupled vehicle–MCA system proposed in Eq. (10). Subsequently, it is shown how to obtain and exploit the eigenstructure of the coupled system in order to obtain a measure of the amount of distortion in each human-perceived quantity as a result of motion filtering.

A. Human-Perceived States from Vehicle Dynamics

To couple the linear vehicle and CWA dynamics, expressions for human-perceived quantities (i.e., specific forces and angular rates) in perturbed form are necessary. To this end, the linear vehicle dynamics are defined first:

$$\delta \dot{x}^p = A^p \delta x^p + B^p \delta u^p$$
$$\delta y^p = C^p \delta x^p + D^p \delta u^p \quad (13)$$

In this formulation, the linear vehicle dynamics are governed by A^p and B^p, with accompanying vehicle state and input vectors δx^p and δu^p, respectively. For aircraft and rotorcraft, the classical formulations of the linear rigid-body dynamics widely applied for stability analysis and flight control system design (see, e.g., [24,25]) can be used directly. For rotorcraft δx^p and δu^p are defined as

$$\delta x^p = \begin{bmatrix} \delta u & \delta v & \delta w & \delta \phi & \delta \theta & \delta p & \delta q & \delta r \end{bmatrix}^T$$
$$\delta u^p = \begin{bmatrix} \delta \theta_0 & \delta \theta_{1_c} & \delta \theta_{1_s} & \delta \theta_{0_{tr}} \end{bmatrix}^T \quad (14)$$

The desired quantities in the vehicle output vector y^p are the perturbed specific forces and rotational rates, i.e.,

$$\delta y^p = \begin{bmatrix} \delta f_x & \delta f_y & \delta f_z & \delta p & \delta q & \delta r \end{bmatrix}^T \quad (15)$$

Comparing Eq. (14) and Eq. (15), it is evident that the perturbed rotational rates are already present in the perturbed state vector. To obtain (linear) expressions for the perturbed specific forces, the vehicle translational equations of motion (see, e.g., [36]) can be used:

$$\dot{V} = f(x^p, u^p) + T_{bi}(\psi, \theta, \phi) g - \omega \times V \quad (16)$$

where $V \equiv \begin{bmatrix} u & v & w \end{bmatrix}^T$ and $f(x^p, u^p) \equiv F_{cg}(x^p, u^p)/m$. Hence, the specific forces appearing in Eq. (16) are the resultant nongravitational forces acting on the vehicle per unit mass. These quantities can also

be expressed in linearized form (see, e.g., [36]). This yields the following generic expression for the linearized specific forces:

$$\delta f_{\square} = \frac{\delta F_{cg}^{\square}}{m} = \square_u \delta u + \square_v \delta v + \square_w \delta w + \square_p \delta p + \square_q \delta q + \square_r \delta r$$
$$+ \square_{\theta_0} \delta\theta_0 + \square_{\theta_{1_c}} \delta\theta_{1_c} + \square_{\theta_{1_s}} \delta\theta_{1_s} + \square_{\theta_{0_{tr}}} \delta\theta_{0_{tr}} \quad (17)$$

where $\square$ is a placeholder for the translational vehicle DOFs. (i.e., X, Y, and Z). Equation (17) expresses the perturbed specific forces as a linear combination of the vehicle states and inputs. Combined with the insight that the vehicle rotational rates appear directly in the state vector, it is possible to specify the C^p and D^p matrices appearing in Eq. (13). These lead directly to the necessary definitions of A^{pm}, B^m, C^{pm}, and D^m appearing in Eq. (10). The reader is referred to [36] for the detailed definitions of these matrices.

B. Extended Eigenvectors of the Coupled System

In Sec. II, the significance of modes to characterize vehicle dynamics was discussed. The eigenvalues of a linear system were shown to reveal information about stability, frequency, and damping of the characteristic vehicle modes. Furthermore, the eigenvector associated with each mode was found to expose the mode shape through the relative magnitude and phase (for complex eigenvalues) between the various states contained in the model. Finally, it was shown that the vehicle response could be described in terms of its modal coordinates, where the MPFs were introduced as a measure of the contribution of each mode in the vehicle's state response. In this subsection, the eigenstructure of the coupled system in Eq. (10) will be used to *quantify* the effect of the MCA dynamics on the existing vehicle modes in terms of human-perceived quantities.

This information can be obtained by applying a modal coordinate transformation to the coupled system. This was outlined in Sec. II and resulted in Eq. (3). In summary, the state vector could be expressed as [see Eq. (2)]:

$$\boldsymbol{x}^c = W^c \boldsymbol{r}^c \quad \text{or} \quad \boldsymbol{r}^c = (W^c)^{-1} \boldsymbol{x}^c \quad (18)$$

where W^c is the modal matrix containing the eigenvectors of the coupled system matrix, i.e., A^c in Eq. (10). Subsequent premultiplication of W^c with the coupled system output matrix C^c from Eq. (10) yields the *extended modal matrix*:

$$C^c W^c = \begin{bmatrix} \boldsymbol{w}_{y^c}^{\lambda_1} & \boldsymbol{w}_{y^c}^{\lambda_2} & \cdots & \boldsymbol{w}_{y^c}^{\lambda_{m-1}} & \boldsymbol{w}_{y^c}^{\lambda_m} \end{bmatrix}$$
$$= \begin{bmatrix} w_{f_x}^{\lambda_1} & w_{f_x}^{\lambda_2} & \cdots & w_{f_x}^{\lambda_{m-1}} & w_{f_x}^{\lambda_m} \\ \vdots & \vdots & & \vdots & \vdots \\ w_{r}^{\lambda_1} & w_{r}^{\lambda_2} & \cdots & w_{r}^{\lambda_{m-1}} & w_{r}^{\lambda_m} \\ w_{f_x^s}^{\lambda_1} & w_{f_x^s}^{\lambda_2} & \cdots & w_{f_x^s}^{\lambda_{m-1}} & w_{f_x^s}^{\lambda_m} \\ \vdots & \vdots & & \vdots & \vdots \\ w_{r^s}^{\lambda_1} & w_{r^s}^{\lambda_2} & \cdots & w_{r^s}^{\lambda_{m-1}} & w_{r^s}^{\lambda_m} \end{bmatrix} \quad (19)$$

From this equation, it can be seen that the C^c matrix scales and combines the right eigenvectors of A^c such that a different set of eigenvectors is obtained, in terms of both the vehicle and CWA-filtered perception states. These *extended* eigenvectors are a linear combination of the original eigenvectors in W^c and, in Eq. (19), are denoted by $\boldsymbol{w}_{y^c}^{\lambda_i}$. The superscript λ_i signifies that the eigenvector corresponds to the ith eigenvalue of the matrix A^c, with $i \in \mathbb{Z}: i \in [1, m]$. Here, m is the number of eigenvalues (i.e., the rank) of matrix A^c. The subscript y^c is used to signify the extended eigenvectors pertaining to the system output vector $\boldsymbol{y}^c$ and distinguishes them from the eigenvectors in W^c pertaining to the coupled system state vector $\boldsymbol{x}^c$. Finally, the quantities $w_{\square}^{\lambda_i}$ denote the extended eigenvector coefficients pertaining to both unfiltered (i.e., vehicle output) and filtered (i.e., motion output)

perception states. The dimension of the extended modal matrix is therefore $12 \times m$ (for 6-DOF motion), where each column is an eigenvector of A^c.

Because of the block triangular structure of the matrix A^c [see Eq. (10)], the m eigenvalues (and eigenvectors) of A^c consist of the n eigenvalues of A^p as well as the k eigenvalues of A^m [38]: $m = n + k$. As noted earlier, the internal dynamics of the CWA effectively *distort* the dynamics of the human-perceived quantities governed by the vehicle dynamics. To quantify this distortion, it is of interest to compare the extended eigenstructures of the uncoupled and (CWA-) coupled vehicle dynamics. This information is readily contained in the extended modal matrix defined in Eq. (19). Namely, of the m eigenvectors in the extended modal matrix, only the n eigenvectors corresponding to the n eigenvalues of A^p are of interest. The remaining k eigenvectors in the extended modal matrix correspond to the eigenvalues of A^m, which capture how the individual dynamic elements in the CWA distort the human-perceived vehicle dynamics. Thus, a new extended modal matrix can be constructed from Eq. (19), which only contains the n eigenvectors corresponding to the eigenvalues of A^p:

$$(C^c W^c)_{*n} = \begin{bmatrix} \boldsymbol{w}_{y^c}^{\lambda_1} & \boldsymbol{w}_{y^c}^{\lambda_2} & \cdots & \boldsymbol{w}_{y^c}^{\lambda_{n-1}} & \boldsymbol{w}_{y^c}^{\lambda_n} \end{bmatrix}$$
$$= \begin{bmatrix} w_{f_x}^{\lambda_1} & w_{f_x}^{\lambda_2} & \cdots & w_{f_x}^{\lambda_{n-1}} & w_{f_x}^{\lambda_n} \\ \vdots & \vdots & & \vdots & \vdots \\ w_{r}^{\lambda_1} & w_{r}^{\lambda_2} & \cdots & w_{r}^{\lambda_{n-1}} & w_{r}^{\lambda_n} \\ w_{f_x^s}^{\lambda_1} & w_{f_x^s}^{\lambda_2} & \cdots & w_{f_x^s}^{\lambda_{n-1}} & w_{f_x^s}^{\lambda_n} \\ \vdots & \vdots & & \vdots & \vdots \\ w_{r^s}^{\lambda_1} & w_{r^s}^{\lambda_2} & \cdots & w_{r^s}^{\lambda_{n-1}} & w_{r^s}^{\lambda_n} \end{bmatrix} \quad (20)$$

where the subscript $*n$ signifies the n columns of $C^c W^c$ in Eq. (19) that correspond to $\lambda_1 \ldots \lambda_n$, i.e., the eigenvalues of A^p. The result in Eq. (20) is the foundation of the proposed EMD methodology, because it allows for the direct comparison of the unfiltered vehicle mode shapes (captured by the coefficients $w_{f_x}^{\lambda_\square}$ through $w_{r}^{\lambda_\square}$) as well as their CWA-filtered equivalents (captured by the coefficients $w_{f_x^s}^{\lambda_\square}$ through $w_{r^s}^{\lambda_\square}$). Consequently, it becomes possible to quantify the degree of modal distortion imposed by the MCA dynamics. In the next section, the utility of the new EMD methodology outlined here will be demonstrated using a case study.

V. Eigenmode Distortion: A Case Study

This section applies the EMD method to a motion cueing evaluation of the 3-DOF hover dynamics of the Bo-105 helicopter (see Fig. 1). First, the visualization of the MCA-induced modal distortion obtained from Eq. (20) will be explained. Subsequently, the effects of changing the break frequency of the high-pass filter in the pitch channel of the CWA will be examined as an example.

A. Visualization of MCA-Induced Modal Distortion

To demonstrate the new EMD methodology, the linear vehicle model is coupled to the CWA dynamics according to Eq. (10). The linearized model of the CWA in Sec. III was derived for the generic 6-DOF case, but is simplified by omitting the lateral CWA channels (i.e., roll, sway, and yaw) in Fig. 4 as well as their corresponding states and outputs from Eqs. (11) and (12). Note that this simplification is done only for the sake of brevity and ease of representation. It does not inhibit the application of the EMD method to 6-DOF vehicle dynamics.

In effect, for the 3-DOF longitudinal case, the extended eigenvector coefficients of interest remaining in Eq. (20) correspond to $\delta f_x^{(s)}$, $\delta f_z^{(s)}$, and $\delta q^{(s)}$. A *modal distortion portrait* illustrates the effect of the MCA on the vehicle's eigenmodes. Figure 5 shows examples of modal distortion portraits pertaining to the MCA-induced distortion
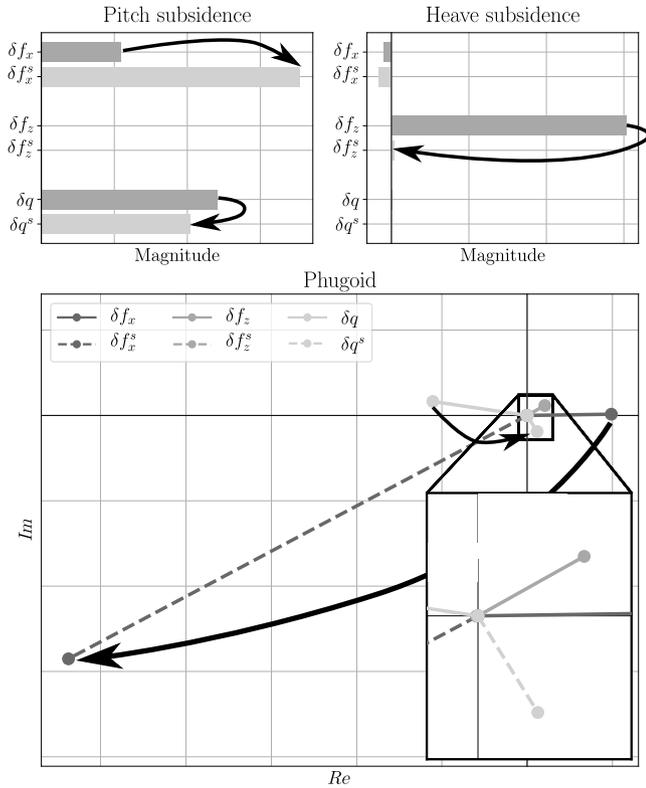
Fig. 5   MCA-induced modal distortion of human-perceived quantities in a 3-DOF linear model of the Bo-105 helicopter in hover.

in each mode of the 3-DOF model of the Bo-105 helicopter. The CWA parameters selected for this example are listed in Table 1. These correspond to the baseline CWA parameters used in [16], with the exception of ζ and $\omega_{1_z^b}$, which were set to values of 0.7071 and 0, respectively.

The distortion of the aperiodic pitch and heave subsidences is represented by a set of horizontal bars, showing the magnitude of both the unfiltered and filtered contributions of the human-perceived quantities. The arrows in the figure indicate the induced modal distortion from the unfiltered (i.e., vehicle) to the filtered (i.e., after MCA) quantities. The distortion of periodic modes is shown in the complex plane and will be discussed in more detail below. Also note that the eigenvectors associated with the dynamic modes are normalized and can be scaled arbitrarily; thus the axes are not labeled.

In the example shown, amplification of δf_x^s with respect to δf_x is seen for both the pitch and heave subsidence modes. This phenomenon is a manifestation of *transient amplification*, i.e., the amplification of the (transient) response by a factor larger than can be expected based on

Table 1   Classical Washout Algorithm parameters used in the EMD case study (filter break frequencies are in rad/s)

Parameter	Value
K_x	0.7
ω_{1_x}	1.0
ω_{2_x}	2.0
K_q	0.7
ω_{3_q}	0.8
K_z	0.5
ω_{1_z}	2.5
$\omega_{1_z^b}$	0
ζ	0.7071

the frequency response [39]. The term is well established in the fields of, e.g., biochemical networks [40] and semiconductor plasmas [41]. In the pitch subsidence mode, attenuation of δq^s with respect to δq is also observed, whereas in the heave subsidence mode δf_z^s is also strongly attenuated with respect to δf_z. This attenuation is expected and is a result of the scaling and high-pass filtering in channels 1 and 3 of the CWA. It is also important to note, however, that these observations reveal nothing about the relative importance of the human-perceived quantities. This is true in particular when comparing $\delta q^{(s)}$ to $\delta f_x^{(s)}$ and $\delta f_z^{(s)}$, because their units differ (i.e., rad/s vs m/s^2). The corresponding modal time traces are also shown in Fig. 6 and, as expected, are consistent with the findings from the modal distortion portraits.

The modal distortion of the periodic phugoid mode is represented in the complex plane, as also shown in Fig. 5. In contrast to aperiodic modes, here the human-perceived quantities are subjected to arbitrary distortions in phase ranging from 0° to 180° in either clockwise (lag) or counterclockwise (lead) directions. From the figure, it is deduced that δf_x^s in the phugoid is affected most by the MCA dynamics, as it shows a phase lag of approximately 135° and is strongly amplified at the same time. The pitch rate δq^s is also strongly affected and shows a phase lead in excess of 90° with respect to δq as well as an attenuation of its amplitude. It also appears that δf_z (in hover) has a limited contribution and that δf_z^s is strongly attenuated to the point where its contribution can no longer be discerned in the phugoid. Again, the corresponding modal time traces are shown in Fig. 6.

Although the modal distortion portraits reveal the effects of the MCA on the individual human-perceived quantities, they also show how the induced distortion affects the relation between these quantities. For example, for the pitch subsidence, δq is seen to dominate the response in terms of its absolute amplitude when compared with δf_x. However, as a result of the MCA, δf_x^s becomes larger in amplitude than δq^s. A similar result is seen in the relation between $\delta q^{(s)}$ and $\delta f_x^{(s)}$ in the phugoid where, as a result of the MCA, the phase lead of δq^s with respect to δf_x^s is reduced from approximately 180° to only 90°. At the same time, the contribution of δf_x^s with respect to δq^s in the phugoid is found to increase substantially.

B.   Sensitivity Study

Dalmeijer et al. [16] exposed an interesting relation between variations in the break frequency of the high-pass filter in the CWA pitch channel and the resulting response of the specific force reproduced in surge. To investigate whether the same effect is observed when EMD is applied, ω_{3_q} as listed in Table 1 is increased and the resulting modal distortion portraits are examined. The most notable results, appearing in the pitch subsidence and phugoid modes, are shown in Fig. 7 for values of ω_{3_q} ranging from 0.8 (baseline) up to 6.0 rad/s. The heave DOF is omitted from the analysis, as the changes in both the heave subsidence mode as well as δf_z^s with varying ω_{3_q} are found negligible.

From Fig. 7b, the most significant effect of increasing ω_{3_q} appears in the MCA-induced distortion of the phugoid mode. For the baseline value of 0.8 rad/s, a strong amplification of the simulated specific force in surge could be distinguished with substantial phase lag. This is also evident from the time responses shown in Fig. 6. As ω_{3_q} is increased, it can be seen that the MCA-induced amplification as well as the phase lag of δf_x^s diminish. For values of ω_{3_q} in excess of 3.0 rad/s, the amplification of the simulated specific force in surge becomes attenuation. The effect on δq^s in the phugoid mode is not shown in the figure because of its strongly diminishing amplitude as ω_{3_q} is increased. However, the phase lag of δq^s with respect to δq is found to reduce from 180° to 90° as ω_{3_q} is increased. In effect, the contributions of δf_x^s and δq^s remaining in the phugoid mode are largely a consequence of the applied tilt coordination in the CWA.

From the EMD analysis discussed thus far, it appears that constraining the rotational vehicle DOF in the MCA is beneficial for reproducing the low-frequency phugoid mode in helicopters. This result is in agreement with the findings from the tailored OMCT analysis in [16]. In EMD, however, the consequence of larger values for ω_{3_q} becomes apparent from the MCA-induced distortion of the
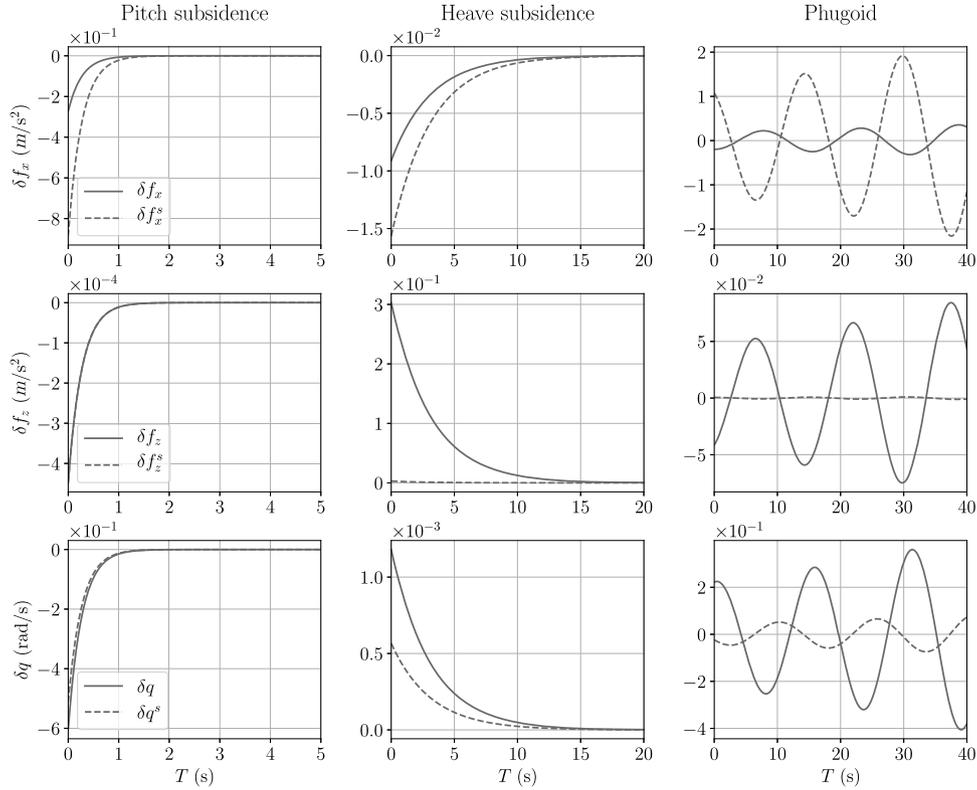
Fig. 6   Time responses corresponding to MCA-induced modal distortion of human-perceived quantities shown in Fig. 5.
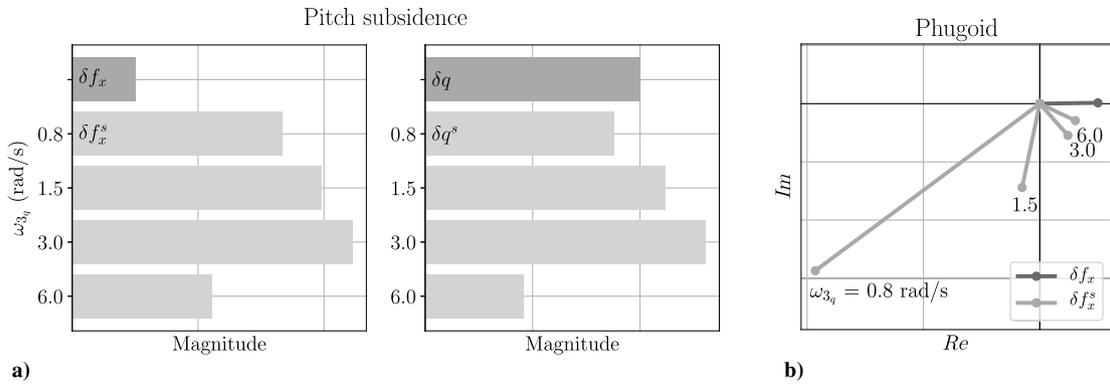

Fig. 7   MCA-induced modal distortion in the a) pitch subsidence (3.7 rad/s) and b) phugoid (0.4 rad/s) modes with increasing ω_{3_q}.

pitch subsidence mode. Namely, as ω_{3_q} is increased up to the approximate value of the frequency of the mode under consideration (i.e., 3.3 rad/s), it is seen from Fig. 7a that the effect is rather limited and even results in a mild amplification of δq^s (i.e., transient amplification). However, as ω_{3_q} is increased beyond 3.0 rad/s, δq^s is found to strongly diminish in amplitude with respect to δq. At the same time, the amplification of δf_x^s with respect to δf_x also becomes smaller. Interestingly, however, the contribution of δf_x^s does remain more than twice as large compared with δf_x even for $\omega_{3_q} = 6.0$ rad/s.

This example shows how an EMD analysis can be used to systematically analyze the coupled dynamics of the simulated vehicle and the MCA. In this case, the analysis leads to the insight that the rotational dynamics of the MCA most strongly affect the longitudinal specific force cue in the phugoid mode. The physical effect of this distorted mode on the actual motion cues experienced by the pilot in the simulator, however, remains rather abstract. Although it is evident that the longitudinal specific force cue is improved as ω_{3_q} is increased (i.e., with attenuation pitch motion cues), there are no intuitive fidelity criteria or boundaries in the modal domain akin to those offered by, e.g., the Sinacori–Schroeder criteria or OMCT. Although

it is possible to define similar boundaries in the modal domain as demonstrated, e.g., for application to haptic feedback systems by Fu et al. [42], this is more complicated for motion cueing fidelity. This is because individual vehicle modes are rarely excited in isolation. Instead, pilot inputs and disturbances typically result in the excitation of multiple modes simultaneously as expressed in Eq. (7). Therefore, knowledge regarding which modes to prioritize in MCA tuning for specific tasks is necessary before meaningful criteria can be defined. A potentially useful metric toward that end is presented in the next section.

VI.   Mode Participation Factor

To quantify the extent to which each mode contributes to the simulated vehicle's overall dynamic response, the MPF can be used. The term was briefly introduced in Sec. II.A. Given a (measured) state vector at time t, $\boldsymbol{x}^p(t)$, the dynamic response can be obtained in terms of the modal coordinates using Eq. (18):

$$\delta \boldsymbol{r}^p(t) = W^{-1}(t)\delta \boldsymbol{x}^p(t) = W^{-1}(t)(\boldsymbol{x}^p(t) - \boldsymbol{x}_e^p(t))$$

Table 2   Classical Washout Algorithm parameters per experimental condition (filter break frequencies are in rad/s)

Parameter	APM	AHM	PHM
K_x	0.3	0.5	0.8
ω_{1_x}	1.25	2.0	1.0
K_z	0.8	1.2	0.2
ω_{1_z}	1.2	0.8	2.0
K_q	1.0	0.5	0.8
ω_{3_q}	0.0	2.0	0.5

Here, $\boldsymbol{x}_e^p(t)$ and $W^{-1}(t)$ are the vehicle state in the linearization point and the inverse modal matrix, respectively, valid at time t. For a maneuver with a duration T, the overall participation of the ith mode can subsequently be formulated as

$$m_i = \int_0^T |r_i^p(t)|\, \mathrm{d}t \quad \forall\ i \in (1, n) \tag{21}$$

where $r_i^p(t)$ are the elements of vector $\delta\boldsymbol{r}^p(t)$ and n are the number of modes. For complex-valued eigenmodes (e.g., the phugoid of an aircraft), $r_i^p(t)$ are complex-valued scalars and appear in conjugate pairs. The overall mode participation of a complex-valued eigenmode is therefore the sum of the two conjugate pairs appearing in $\delta\boldsymbol{r}^p(t)$.

An illustrative example of the use of MPFs can be found in Miletović et al. [30]. Here, a preliminary experiment is documented to evaluate EMD-based motion cueing configurations tailored to each mode in the 3-DOF longitudinal dynamics of the AH-64 helicopter in hover. This yielded three motion cueing configurations, namely, pitch subsidence motion (APM), heave subsidence motion (AHM), and phugoid motion (PHM). The CWA parameters and corresponding values for each condition are included in Table 2. In addition to

these three configuration, a no-motion (NM) configuration was also incorporated in the experiment.

All motion cueing configuration were evaluated with two helicopter test pilots on the SIMONA Research Simulator at TU Delft, The Netherlands. The pilots were asked to perform the precision hover mission task element (MTE) from [19] in the presence of turbulence, with each repetition of the task lasting approximately 30 s. The reader is referred to [30] for further details on the individual motion cueing configurations as well as the experimental setup. In this paper, only the measured task performances and MPFs are further discussed.

Figure 8 shows the MPFs for each motion cueing configuration evaluated. From the figure, it can be seen that the measured MPFs vary substantially across the experimental conditions and between the two pilots. When considering the *median* MPFs corresponding to each motion configuration, however, the relative contribution of each mode remains approximately constant. The phugoid mode appears to dominate the vehicle response in all conditions, followed by the pitch and heave subsidences, respectively. Another common result is that the phugoid and pitch subsidence MPFs are larger in condition AHM than in the other conditions. This could indicate that the excitation of these modes is stronger when pitch and surge motion cues are absent. This is not corroborated by the MPFs corresponding to the NM condition of pilot 1, which are remarkably small in comparison to the other conditions with motion.

Figure 9 shows the accompanying task performance in terms of longitudinal and vertical position root-mean-square (RMS) error. Interestingly, from this figure, it is apparent that the stronger excitation of the phugoid and pitch subsidence modes in condition AHM does not necessarily translate to a larger longitudinal position RMS as compared with the other conditions. On the other hand, for pilot 2 in particular, there seems to be a strong relation between substantially smaller longitudinal and vertical position RMSs and generally smaller MPFs in condition APM. Although the MPFs in condition APM for pilot 1 are similar to those for pilot 2, a smaller position RMS compared with the other conditions is only observed in the vertical direction.
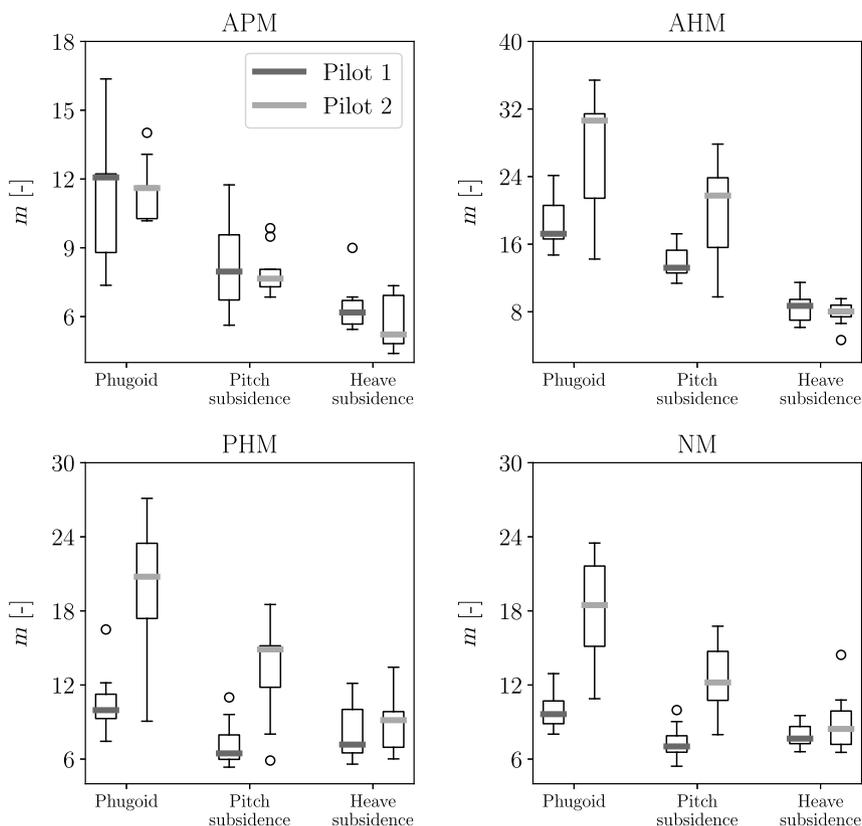

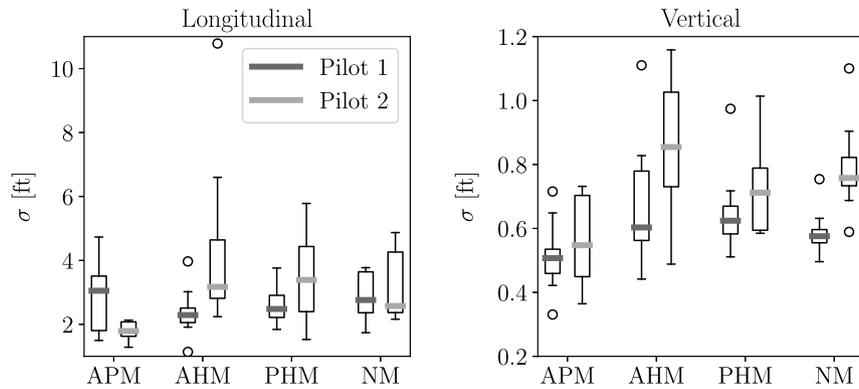**Fig. 8   Mode participation factors per experimental condition.**

Fig. 9 Horizontal and vertical position RMS's per experimental condition.

Although inconclusive in terms of the relative favorability of the three different motion configurations evaluated, these results do highlight some interesting properties of the MPF. For example, the median MPFs suggest a constant relative distribution of the individual modes' overall contributions across the evaluated motion conditions and pilots. In addition, there is some evidence that measured MPFs are correlated with the motion cues present in the different simulator DOFs, a result also corroborated by other experiments performed to date [31,32,36]. As such, knowledge of the MPFs can potentially facilitate targeted EMD-based tuning of the MCA for specific maneuvers and tasks.

VII. Discussion

EMD constitutes a new perspective on motion cueing fidelity in vehicle simulation. It relies on linear(ized) and subsequently coupled mathematical models of the simulated vehicle and the MCA, which enable the application of modal analysis to quantify the distortion of the vehicle's characteristic modes of motion due to the dynamics of the MCA. Compared with existing methods, such as the Sinacori–Schroeder criteria and the OMCT, a more in-depth understanding about the effect of the MCA on the simulated vehicle's perceived dynamics can be obtained.

A case study revealed the effect of couplings between the different simulator DOFs in the MCA that are not directly apparent from other methods, such as the OMCT [16]. This is true particularly for the surge and pitch DOFs and highlights the role of the various MCA parameters in relation to the simulated vehicle dynamics. In part, these insights can be attributed to the ability of EMD to account for the *transient* vehicle and MCA responses [39] as opposed to only the *steady-state* responses assumed in OMCT.

The paper also addressed how EMD enables targeted tuning of the MCA for arbitrary vehicle dynamics and their associated dynamic modes, most notably through the use of MPFs. This was exemplified using earlier work, i.e., [30], from which notable results pertaining to MPFs were briefly highlighted. In this study, EMD was used to tune the MCA in order to portray the longitudinal dynamic modes of a helicopter in hover, after which the resulting configurations were evaluated using a preliminary pilot-in-the-loop experiment in a motion-base flight simulator. Interestingly, the measured MPFs, though subject to substantial variance across runs and pilots, show a constant distribution of the participation of each mode in the measured dynamic response. Moreover, there appears to be a relation between the presence (or absence) of motion cues and the measured MPF magnitudes. These results suggest that the MPF can serve as a vital bridge between the task and the modal domain in which EMD operates. For example, for rotorcraft, one could study typical MTEs used in the evaluation of handling qualities [19] to determine the modes that dominate the dynamic response. Subsequently, EMD can be applied to tailor motion cues to these specific modes [36]. This is especially interesting for applications involving handling qualities evaluations, where motion cues tailored to specific modes could better support the pilots' assessment of the vehicle's handling qualities.

In other recent studies, namely, [31,32], EMD was also used to tune the MCA to portray a fixed-wing aircraft's short period and Dutch roll modes for a pitch attitude capture and a yaw disturbance rejection task, respectively. Both studies also report pilot-in-the-loop experiments, where the EMD-based configurations were evaluated and compared with configurations obtained using other motion tuning strategies. To date, the results from these various experiments suggest that pilots do not generally favor EMD-based motion settings subjectively over, e.g., OMCT-based motion settings. On the other hand, there is evidence that EMD-based motion tailored to portray specific dynamic modes results in an improved suppression of the respective (undesired) modes' contribution to the measured vehicle response (i.e., lower MPFs) [32]. The latter further reinforces the synergistic utility of MPFs to bridge the gap between the task and a quantitative motion cueing fidelity analysis based on EMD.

Nonetheless, like OMCT, EMD represents MCA-induced motion distortion in a rather abstract and, barring relative dimensions between human-perceived quantities, essentially dimensionless domain. Although abstraction is necessary to permit the systematic analysis that the EMD method offers, it also means that the severity of certain motion distortions cannot be judged directly from the perspective of the human operator, i.e., by including human perceptual limitations. To partly alleviate this limitation, an extension to EMD where the extended eigenvectors of the coupled system are scaled using human perception thresholds has been proposed [32]. EMD also requires that linear models of both the simulated vehicle and MCA dynamics are available, which may not be straightforward in some applications (e.g., training simulators, adaptive MCAs). This does not mean that EMD has no value for such applications, however. For example, EMD could still be used to define more representative OMCT input signals that better capture typical interactions between DOFs present in the vehicle dynamics. OMCT tests that stimulate multiple DOFs, such as the pitch tests, could be refined to better capture typical vehicle dynamics, based on insights from EMD. For applications where vehicle and MCA models are readily available and where modal analysis better aligns with established practice (e.g., flying and handling qualities research/ evaluation), EMD is likely more applicable than existing methods. For the moment, EMD still lacks intuitive criteria or boundaries by which to assess motion fidelity akin to, e.g., the Sinacori–Schroeder criteria and the more recent OMCT criteria. In time, these could be determined using MPF distributions across a wide range of different tasks.

Future work is primarily aimed at further investigating the utility of the EMD method, in conjunction with MPFs, for task-specific MCA tuning, as well as accommodating applications to other vehicle types.

VIII. Conclusions

This paper introduced EMD as a novel methodology to analyze the intricate interaction between the simulated vehicle and MCA dynamics in motion-base simulators. EMD relies on the application of modal analysis to an algebraically coupled system containing both the vehicle and MCA dynamics in linear(ized) form. The effect of the MCA is quantified as the distortion of the coupled system's eigenvectors

expressed in terms of human-perceived quantities (i.e., angular rate and specific force) in each of the simulated vehicle modes.

A case study involving helicopter dynamics was used to demonstrate the applicability of the method and to highlight the key insights that can be gained from EMD. Most notably, it was shown that the pitch dynamics of the MCA strongly affect the longitudinal specific force cue in the phugoid mode. This relation is not as apparent from other, existing methods for motion fidelity evaluation such as the OMCT.

The paper furthermore introduced the MPF as a metric to capture the extent to which individual vehicle modes contribute to the (measured) state response. Results from a preliminary experiment were used to demonstrate the utility of the metric and suggest that a correlation exists between MPFs and the presence of motion cues in the different simulator DOFs. Together, EMD and MPFs therefore constitute a systematic and model-based framework to facilitate tuning and evaluation of MCAs.

References

[1] Anon., "Certification Specifications for Helicopter Flight Simulation Training Devices (CS-FSTD (H)), Initial Issue," European Aviation Safety Agency, Tech. Rept., 2012, https://www.easa.europa.eu/sites/default/files/dfu/CS-FSTD%28H%29%20Initial%20Issue.pdf [retrieved Jan. 2021].

[2] Sinacori, J. B., "The Determination of Some Requirements for a Helicopter Research Simulation Facility," Systems Technology, Inc., NASA-CR-152066, Sept. 1977.

[3] Schroeder, J. A., "Helicopter Flight Simulation Motion Platform Requirements," NASA TP-1999-208766, Moffett Field, CA, July 1999.

[4] Advani, S. K., and Hosman, R. J. A. W., "Towards Standardizing High-Fidelity Cost-Effective Motion Cueing in Flight Simulation," *Proceedings of the Royal Aeronautical Society Flight Simulation Conference*, London, Nov. 2006, pp. 87–102.

[5] Advani, S. K., and Hosman, R. J. A. W., "Revising Civil Simulator Standards—An Opportunity for Technological Pull," *Proceedings of the AIAA Modeling and Simulation Technologies Conference and Exhibit*, AIAA Paper 2006-6248, Aug. 2006.
https://doi.org/10.2514/6.2006-6248

[6] Advani, S. K., Hosman, R. J. A. W., and Potter, M., "Objective Motion Fidelity Qualification in Flight Training Simulators," *AIAA Modeling and Simulation Technologies Conference and Exhibit, Hilton Head, South Carolina*, AIAA Paper 2007-6802, Aug. 2007.
https://doi.org/10.2514/6.2007-6802

[7] Anon., "ICAO 9625: Manual of Criteria for the Qualification of Flight Simulation Training Devices. Volume 1: Aeroplanes," 3rd ed., International Civil Aviation Authority, Tech. Rept., ICAO Doc. 9625, Vol. I, 2009.

[8] Hosman, R. J. A. W., and Advani, S. K., "Design and Evaluation of the Objective Motion Cueing Test and Criterion," *Aeronautical Journal*, Vol. 120, No. 1227, 2016, pp. 873–891.
https://doi.org/10.1017/aer.2016.35

[9] Anon., "Flight Simulation Training Device Initial and Continuing Qualification and Use," Federal Aviation Authorities, Tech. Rept. 14 CFR Part-60, 2016, https://www.faa.gov/about/initiatives/nsp/media/14cfr60_searchable_version.pdf [retrieved Jan. 2021].

[10] Stroosma, O., van Paassen, M. M., Mulder, M., Hosman, R. J. A. W., and Advani, S. K., "Applying the Objective Motion Cueing Test to a Classical Washout Algorithm," *Proceedings of the AIAA Modeling and Simulation Technologies Conference*, AIAA Paper 2013-4834, Aug. 2013.
https://doi.org/10.2514/6.2013-4834

[11] Seehof, C., Durak, U., and Duda, H., "Objective Motion Cueing Test–Experiences of a New User," *Proceedings of the AIAA Modeling and Simulation Technologies Conference*, AIAA Paper 2014-2205, Jun. 2014.
https://doi.org/10.2514/6.2014-2205

[12] Zaal, P. M. T., Schroeder, J. A., and Chung, W. W. Y., "Transfer of Training on the Vertical Motion Simulator," *Proceedings of the AIAA Modeling and Simulation Technologies Conference*, AIAA Paper 2014-2206, Jun. 2014.
https://doi.org/10.2514/6.2014-2206

[13] Zaal, P., Schroeder, J., and Chung, W., "Objective Motion Cueing Criteria Investigation Based on Three Flight Tasks," *Aeronautical Journal*, Vol. 121, No. 1236, 2017, pp. 163–190.
https://doi.org/10.1017/aer.2016.119

[14] Jones, M., "Motion Cueing Optimisation Applied to Rotorcraft Flight Simulation," *CEAS Aeronautical Journal*, Vol. 8, No. 3, 2017, pp. 523–539.
https://doi.org/10.1007/s13272-017-0256-1

[15] Jones, M., "A Method for Automatic Tuning of Flight Simulator Motion Platforms," *International Journal of Modeling, Simulation, and Scientific Computing*, Vol. 8, No. 4, 2017, Paper 1743004.
https://doi.org/10.1142/S1793962317430048

[16] Dalmeijer, W., Miletović, I., Stroosma, O., and Pavel, M. D., "Extending the Objective Motion Cueing Test to Measure Rotorcraft Simulator Motion Characteristics," *Proceedings of the AHS 73rd Annual Forum*, American Helicopter Soc., Fairfax, VA, May 2017, pp. 1876–1891.

[17] Harper, R. P., and Cooper, G. E., "Handling Qualities and Pilot Evaluation," *Journal of Guidance, Control, and Dynamics*, Vol. 9, No. 5, 1986, pp. 515–529.
https://doi.org/10.2514/3.20142

[18] Anon., "Military Specification: Flying Qualities of Piloted Airplanes," MIL-F-8785C, United States Army, Tech. Rept., 1980.

[19] Anon., "Aeronautical Design Standard—Performance Specification—Handling Qualities Requirements for Military Rotorcraft," US Army AMCOM Tech. Rept. ADS-33E-PRF, Redstone, AL, March 2000.

[20] Amirouche, M. L., and Huston, R. L., "Collaborative Techniques in Modal Analysis," *Journal of Guidance, Control, and Dynamics*, Vol. 8, No. 6, 1985, pp. 782–785.
https://doi.org/10.2514/3.20055

[21] Kao, C. K., and Sinha, A., "Coupled Modal Sliding Mode Control of Vibration in Flexible Structures," *Journal of Guidance, Control, and Dynamics*, Vol. 15, No. 1, 1992, pp. 65–72.
https://doi.org/10.2514/3.20802

[22] Liu, Z.-s., Wang, D.-j., Hu, H.-c., and Yu, M., "Measures of Modal Controllability and Observability in Vibration Control of Flexible Structures," *Journal of Guidance, Control, and Dynamics*, Vol. 17, No. 6, 1994, pp. 1377–1380.
https://doi.org/10.2514/3.21363

[23] Taira, K., Brunton, S. L., Dawson, S. T. M., Rowley, C. W., Colonius, T., McKeon, B. J., Schmidt, O. T., Gordeyev, S., Theofilis, V., and Ukeiley, L. S., "Modal Analysis of Fluid Flows: An Overview," *AIAA Journal*, Vol. 55, No. 12, 2017, pp. 4013–4041.
https://doi.org/10.2514/1.J056060

[24] Cook, M., *Flight Dynamics Principles: A Linear Systems Approach to Aircraft Stability and Control*, Aerospace Engineering, Elsevier Science, Amsterdam, 2013.

[25] Padfield, G. D., *Helicopter Flight Dynamics: The Theory and Application of Flying Qualities and Simulation Modelling*, 2nd ed., Blackwell Publ., Oxford, U.K., 2007.

[26] Sobel, K. M., and Lallman, F. J., "Eigenstructure Assignment for the Control of Highly Augmented Aircraft," *Journal of Guidance, Control, and Dynamics*, Vol. 12, No. 3, 1989, pp. 318–324.
https://doi.org/10.2514/3.20411

[27] Low, E., and Garrard, W. L., "Design of Flight Control Systems to Meet Rotorcraft Handling Qualities Specifications," *Journal of Guidance, Control, and Dynamics*, Vol. 16, No. 1, 1993, pp. 69–78.
https://doi.org/10.2514/3.11429

[28] Liu, G. P., and Patton, R., *Eigenstructure Assignment for Control System Design*, Wiley, New York, 1998.

[29] Reid, L. D., and Nahon, M. A., "*Flight Simulation Motion-Base Drive Algorithms. Part 1: Developing and Testing the Equations,*" Univ. of Toronto, Inst. for Aerospace Studies Tech. Rept. UTIAS 296, Dec. 1985.

[30] Miletović, I., Pavel, M. D., Stroosma, O., Pool, D. M., van Paassen, M. M., Wentink, M., and Mulder, M., "Eigenmode Distortion as a Novel Criterion for Motion Cueing Fidelity in Rotorcraft Flight Simulation," *Proceedings of the 44th European Rotorcraft Forum*, ERF Paper 45, NLR, Amsterdam, Sept. 2018, pp. 1–12, https://dspace-erf.nlr.nl/xmlui/handle/20.500.11881/3956.

[31] Stoev, S., van Paassen, M. M., Stroosma, O., Miletović, I., and Mulder, M., "Eigenmode Distortion Analysis for Motion Cueing Evaluation in Fixed-Wing Aircraft Simulators," *Proceedings of the AIAA Modeling and Simulation Technologies Conference*, AIAA Paper 2019-0179, Jan. 2019.
https://doi.org/10.2514/6.2019-0179

[32] Tillema, G. H. J., Stroosma, O., Miletović, I., and Mulder, M., "Perceptual Eigenmode Distortion Analysis for Motion Cueing Evaluation in Fixed-Wing Aircraft Simulators," *Proceedings of the AIAA Modeling and Simulation Technologies Conference*, AIAA Paper 2021-1012, Jan. 2021.
https://doi.org/10.2514/6.2021-1012

[33] Oppenheim, A. V., and Verghese, G. C., *Signals, System and Inference*, Pearson, London, U.K., 2015.

[34] Hosman, R., and Stassen, H. G., "Pilot's Perception and Control of Aircraft Motions," *7th IFAC Symposium on Analysis, Design and Evaluation of Man Machine Systems (MMS'98)*, Vol. 31, International Federation of Automatic Control (IFAC), Laxenburg, Austria, Sept. 1998, pp. 311–316.
https://doi.org/10.1016/S1474-6670(17)40111-X

[35] Previc, F. H., and Ercoline, W. R., *Spatial Disorientation in Aviation*, AIAA, Reston, VA, 2004.

[36] Miletović, I., "Motion Cueing Fidelity in Rotorcraft Flight Simulation: A New Perspective Using Modal Analysis," Ph.D. Thesis, Faculty of Aerospace Engineering, Delft Univ. of Technology, Delft, The Netherlands, Feb. 2020. https://doi.org/10.4233/uuid:4fdea178-a5b1-4620-987e-b1f2f9c23d32

[37] Grant, P. R., "The Development of a Tuning Paradigm for Flight Simulator Motion Drive Algorithms," Ph.D. Thesis, Inst. for Aerospace Studies, Univ. of Toronto, Toronto, Canada, 1996.

[38] Strang, G., *Linear Algebra and Its Applications*, Thomson, Brooks/Cole, Belmont, CA, 2006, Chap. 5.

[39] van Donge, H., "Motion Cueing Tuning and Evaluation in CH-47 Helicopter Simulation Using the Eigenmode Distortion Method," Master's Thesis, Delft Univ. of Technology, Delft, The Netherlands, 2020.

[40] Dixon, J., Lindemann, A., and McCoy, J. H., "Transient Amplification Limits Noise Suppression in Biochemical Networks," *Physical Review E*, Vol. 93, 2016, Paper 012415. https://doi.org/10.1103/PhysRevE.93.012415

[41] Dubey, S., Paliwal, A., and Ghosh, S., "Transient Amplification Characteristics of Frequency Modulated Wave in Semiconductor Plasmas," *Chinese Journal of Physics*, Vol. 61, Oct. 2019, pp. 227–234. https://doi.org/10.1016/j.cjph.2019.08.010

[42] Fu, W., Van Paassen, M. M., and Mulder, M., "Human Threshold Model for Perceiving Changes in System Dynamics," *IEEE Transactions on Human-Machine Systems*, Vol. 50, No. 5, Oct. 2020. https://doi.org/10.1109/THMS.2020.2989383